

# IRSSG: An Open-Source Software Package for Spin Space Groups

Sheng Zhang,<sup>1,2,\*</sup> Ziyin Song,<sup>1,2,\*</sup> Zhong Fang,<sup>1,2</sup> Hongming Weng,<sup>1,3</sup> and Zhijun Wang<sup>1,3,†</sup>

<sup>1</sup>*Beijing National Laboratory for Condensed Matter Physics,  
and Institute of Physics, Chinese Academy of Sciences, Beijing 100190, China*

<sup>2</sup>*University of Chinese Academy of Sciences, Beijing 100049, China*

<sup>3</sup>*Condensed Matter Physics Data Center, Chinese Academy of Sciences, Beijing 100190, China*

(Dated: December 1, 2025)

We present an open-source software package IRSSG for investigating magnetic systems with spin space groups (SSGs). The package works within the density functional theory (DFT) framework and requires wavefunctions from DFT codes, such as VASP, Quantum ESPRESSO, as well as any other code that has an interface to Wannier90. We introduce a set of compact SSG international symbols by combining non-crystallographic point groups with the 230 crystallographic space groups. The program first identifies all SSG operations and determines the SSG international symbol for a given magnetic system. It then generates the SSG character tables of little groups at any  $k$  point. Finally, it computes the traces of matrix presentations of SSG operations and assigns irreducible corepresentation labels to magnetic energy bands. The program is not only timely but also essential for advancing research on the study of magnons, altermagnetism, magnetic topology, and novel high-degeneracy excitations in SSG systems.

## Program summary

*Program title:* IRSSG

*Program Files doi:* tobeupdated

*Licensing provisions:* GNU Lesser General Public License, <https://www.gnu.org/licenses/lgpl-3.0.html#license-text>

*Programming language:* Python 3, Fortran 90

*Nature of problem:* Determining the irreducible (co)representations of band structures under spin space groups (SSGs) is particularly valuable for band-character assignment, connectivity analysis, and topology diagnostics in SSG systems.

*Solution method:* The program identifies all SSG operations and determines the corresponding SSG international symbol. It constructs the  $k$ -little-group character tables using the Hamiltonian method, and determines the band irreducible (co)representations by comparing the traces of matrix representations of SSG operations acting on DFT wavefunctions or Wannier tight-binding states.

## I. INTRODUCTION

Symmetry plays a fundamental role in condensed matter and materials physics by facilitating the prediction of emergent phenomena and material properties, such as ferroelectricity [1–3], phonons [4–6], topological insulators [7–10], and superconductivity [11–13]. Symmetry also provides powerful constraints that significantly simplify otherwise complex many-body problems. For crystals, the symmetries are categorized into 230 crystallographic space groups (CSGs). In magnetic materials, a variety of spin configurations (*e.g.*, ferromagnetic, antiferromagnetic, and helical orders) can emerge. To describe such materials in the presence of spin–orbit coupling (SOC), the time-reversal operation  $\mathcal{T}$  is combined with the 230 CSGs, resulting in 1651 Shubnikov magnetic space groups (MSGs) [14]. However, in the weak-SOC regime relevant for magnetic materials and magnons, the spin and lattice degrees of freedom decouple, leading to a richer symmetry structure. Therefore, Brinkman and Elliott introduced the concept of spin space groups (SSGs), where spin and lattice operations are treated individually, without being rigidly tied [15]. Recently, physicists have employed various methodologies to achieve a comprehensive enumeration and classification of SSGs [16–18].

The SSGs are now widely used in the analysis of topological electronic bands, magnon spectra [19, 20], superconducting order parameters [21], altermagnetism [22, 23], anomalous Hall responses [24], *etc.* Jiang *et al.* systematically enumerated all such SSGs, including 1,421 collinear groups, 24,788 coplanar noncollinear groups, and 157,289 non-coplanar groups, in which the magnetic primitive cell is at most twelve times the atomic primitive cell [18]. However, a set of compact and intuitive SSG international symbols is still lacking.

\*These authors contributed equally to this work.

†Electronic address: [zjwang11@hotmail.com](mailto:zjwang11@hotmail.com);

The codes are available in the public repository: <https://github.com/zjwang11/IRSSG/>.

For nonmagnetic and magnetic topological materials, the program **IRVSP** [25] represents the first computational tool capable of determining irreducible (co)representations [(co)irreps] and uncovering the band topology of electronic band structures computed using density functional theory (DFT) codes such as VASP [26, 27], Quantum ESPRESSO [28, 29], as well as any other code that has an interface to Wannier90 [30, 31]. It can generate the input files needed to calculate elementary band representations and symmetry-based indicators via the **TopMat** server [32]. Within this band-representation framework, methods have also been developed to diagnose unconventional materials with obstructed atomic limit via the **BRdecomp** server [33]. In this work, we develop **IRSSG** to obtain the SSG coirreps of the band structures of magnetic materials with arbitrary SSG symmetries for the first time. **IRSSG** identifies all SSG operations and determines the SSG number and international symbol. Meanwhile, we introduce a set of compact SSG international symbols by combining non-crystallographic point groups with the 230 crystallographic space groups.

The paper is structured as follows. In Sec. II, we present the methods implemented in our program, including the basic concepts of SSGs as well as the method to construct coirreps based on SSG operations and to obtain matrix presentations of materials. In Sec. III, the general workflow of the **IRSSG** code is described in detail. The capabilities of **IRSSG** are described in Sec. IV. In Sec. V, we introduce the installation steps and usage of the program. Some typical examples are shown in Sec. VI.

## II. BASIC CONCEPTS OF SPIN SPACE GROUPS AND COIRREPS

### A. Spin space groups and international symbols

Given a magnetic crystal structure with atoms  $\{\mathbf{s}_i, \mathbf{r}_i, X_i\}$ , SSG operations are defined as

$$\begin{aligned} \mathcal{G} &= \{\mathcal{O}_\alpha \equiv \{U_\alpha | R_\alpha | \mathbf{v}_\alpha\} | U_\alpha \mathbf{s}_i = \mathbf{s}_j, R_\alpha \mathbf{r}_i + \mathbf{v}_\alpha = \mathbf{r}_j, X_i = X_j\}, \\ U_\alpha &\in O(3), \quad \det(U_\alpha) = \begin{cases} +1, & \mathcal{O}_\alpha \text{ is unitary without } \mathcal{T}, \\ -1, & \mathcal{O}_\alpha \text{ is anti-unitary with } \mathcal{T}, \end{cases} \\ R_\alpha &\in O(3), \quad \det(R_\alpha) = \begin{cases} +1, & R_\alpha \text{ is a proper rotation without } \mathcal{I}, \\ -1, & R_\alpha \text{ is an improper rotation with } \mathcal{I}. \end{cases} \end{aligned} \quad (1)$$

Here  $\mathbf{s}_i$ ,  $\mathbf{r}_i$ , and  $X_i$  are the magnetic moment, position, and element type of the  $i$ th atom, respectively. An SSG operation is denoted as  $\mathcal{O}_\alpha = \{U_\alpha | R_\alpha | \mathbf{v}_\alpha\}$ , consisting of a spin part  $U_\alpha$  and a lattice part  $\{R_\alpha | \mathbf{v}_\alpha\}$ . The time-reversal ( $\mathcal{T}$ ) symmetry reverses the spin direction and acts as an ‘inversion’ symmetry in spin space. Therefore,  $\det(U_\alpha) = -1$  indicates the presence of  $\mathcal{T}$ . The  $\det(R_\alpha) = -1$  indicates the presence of inversion ( $\mathcal{I}$ ), resulting in an improper rotation. In an SSG, the spin rotation  $U_\alpha$  and lattice rotation  $R_\alpha$  are  $O(3)$  matrices and independent. In a sense, the 230 CSGs and 1651 MSGs are special cases of SSGs. Explicitly, a CSG is an SSG with  $U_\alpha = E$  for all  $\mathcal{O}_\alpha \in \mathcal{G}$ , while an MSG is an SSG with  $U_\alpha = \pm R_\alpha$  for all  $\mathcal{O}_\alpha \in \mathcal{G}$ . Therefore, although **IRSSG** is developed for SSGs, it can also work for the 230 CSGs and 1651 MSGs, as long as the operations are given properly.

In general, a special subgroup of  $\mathcal{G}$  is defined as the spin-only group,

$$\begin{aligned} \mathcal{S}_0 &\equiv \{\mathcal{O}_\alpha \in \mathcal{G} | \{R_\alpha | \mathbf{v}_\alpha\} = \{E | \mathbf{0}\}\}, \quad \mathcal{G}_0 = \mathcal{G} / \mathcal{S}_0, \\ \mathcal{G} &= \mathcal{S}_0 \times \mathcal{G}_0 \end{aligned} \quad (2)$$

which contains the SSG operations whose lattice part is the identity. Since the coset representatives of  $\mathcal{G} / \mathcal{S}_0$  form a group ( $\mathcal{G}_0$ ),  $\mathcal{G}$  can be expressed as a direct product of  $\mathcal{S}_0$  and  $\mathcal{G}_0$ . According to the magnetic configuration, SSGs can be classified into three types: collinear (I), coplanar (II) and noncoplanar (III), each corresponding to a specific spin-only group, as shown in Table I. We now introduce two groups derived from  $\mathcal{G}_0$ : the spin part group  $\mathcal{P}$  and the lattice part group  $\mathcal{H}$ ,

$$\mathcal{P} \equiv \{U_\alpha | \forall \mathcal{O}_\alpha \in \mathcal{G}_0\}, \quad \mathcal{H} \equiv \{\{R_\alpha | \mathbf{v}_\alpha\} | \forall \mathcal{O}_\alpha \in \mathcal{G}_0\}. \quad (3)$$

Clearly,  $\mathcal{P}$  belongs to an NPG, while  $\mathcal{H}$  belongs to a CSG. Thus, any SSG operation of  $\mathcal{G}_0$  can be expressed by an element ( $\mathbf{x}$ ) of  $\mathcal{H}$ , with a superscript element ( $\delta$ ) of  $\mathcal{P}$  (*i.e.*,  $\mathbf{x}^\delta \equiv \{\delta | \mathbf{x}\}$ ).

Based on the above analysis of the SSG group structure, we propose a set of compact and intuitive SSG international symbols by the following steps: (1) identify the type of magnetic configuration (I: collinear; II: coplanar; III: noncoplanar); (2) identify the spin part group  $\mathcal{P}$  (third column of Table I); (3) identify the lattice part group  $\mathcal{H}$  with the international symbol  $Xxyz$ . The typical translations of the Bravais-lattice type  $X$  and the rotations  $x, y, z$  are the generators of  $\mathcal{H}$ ; (4) find  $\alpha, \beta, \gamma$  elements of  $\mathcal{P}$  combined with three typical translational generators; (5) find  $\delta / \epsilon / \eta$

Table I: Spin space groups and international symbols. The non-crystallographic point group  $\mathcal{P}$  (in Schönflies notation), is the group formed by the spin parts of the elements of  $\mathcal{G}_0$  in Eq. (3). Its elements are listed as  $\alpha, \beta, \gamma, \delta$ , *et al.*, denoted in Hermann–Mauguin notation. The crystallographic space group  $\mathcal{H}$  is the group formed by the lattice parts of  $\mathcal{G}_0$  in Eq. (3), whose international notation is Xyz. X stands for the Bravais-lattice type and x/y/z are the Hermann–Mauguin symbols of the rotational generators. A compact SSG international symbol can be expressed in the form of  $X^{\alpha,\beta,\gamma}x^\delta y^\epsilon z^\eta (\mathcal{P}^{I/II/III})$ .

Spin space group $\mathcal{G}$ and international symbol $X^{\alpha,\beta,\gamma}x^\delta y^\epsilon z^\eta (\mathcal{P}^{I/II/III})$ ( $\mathcal{G} = \mathcal{S}_0 \times \mathcal{G}_0$ )					
Magnetic Configuration	Spin-only group $\mathcal{S}_0$	Group $\mathcal{G}_0$			
		$\mathcal{P}$ (spin part) ( $\mathcal{P} \equiv \{\alpha, \beta, \gamma, \delta, \dots\}$ )	$\mathcal{H}$ (lattice part)		$\mathcal{G}_0$ generators
I: Collinear	$\{\{C_{\infty z}  E \mathbf{0}\}, \{M_x C_{\infty z}  E \mathbf{0}\}\}$	$C_1, C_i$	X : $\mathbf{a}_1, \mathbf{a}_2, \mathbf{a}_3$	x/y/z	$X^{\alpha,\beta,\gamma}$ $x^\delta$
II: Coplanar	$\{\{E  E \mathbf{0}\}, \{M_z  E \mathbf{0}\}\}$	$C_1, C_i, C_s, C_n, C_{nv}$ ( $n \geq 2$ )	P: 100, 010, 001 C: $\frac{1}{2}\frac{1}{2}0, \frac{1}{2}\frac{1}{2}0, 001$ I: $\frac{1}{2}\frac{1}{2}\frac{1}{2}, \frac{1}{2}\frac{1}{2}\frac{1}{2}, \frac{1}{2}\frac{1}{2}\frac{1}{2}$ A: 100, $0\frac{1}{2}\frac{1}{2}, 0\frac{1}{2}\frac{1}{2}$ F: $0\frac{1}{2}\frac{1}{2}, \frac{1}{2}0\frac{1}{2}, \frac{1}{2}\frac{1}{2}0$ R: $\frac{2}{3}\frac{1}{3}\frac{1}{3}, \frac{1}{3}\frac{2}{3}\frac{1}{3}, \frac{1}{3}\frac{1}{3}\frac{2}{3}$	1, $\bar{1}$ , 2, 2 $_1$ , 3, $\bar{3}$ , 3 $_1$ , 3 $_2$ , 4, $\bar{4}$ , 4 $_1$ , 4 $_2$ , 4 $_3$ , 6, $\bar{6}$ , 6 $_1$ , 6 $_2$ , 6 $_3$ , 6 $_4$ , 6 $_5$ , a, b, c, d, e, m, n	$\{\alpha  E \mathbf{a}_1\}$ , $\{\beta  E \mathbf{a}_2\}$ , $\{\gamma  E \mathbf{a}_3\}$
III: Noncoplanar	$\{\{E  E \mathbf{0}\}\}$	$C_1, C_i, C_s, C_n, C_{nv}, C_{nh}, S_{2n}, D_n, D_{nh}, D_{nd}, T, T_h, T_d, O, O_h, I, I_h$			

element in  $\mathcal{P}$  combined with the rotational generators x/y/z of  $\mathcal{H}$ . Thus, an SSG international symbol is given by  $X^{\alpha,\beta,\gamma}x^\delta y^\epsilon z^\eta (\mathcal{P}^{I/II/III})$ . The redefined spin-space coordinates are output, depending on the spin configuration provided in a magnetic crystal structure. For example, the SSG international symbol of  $\text{Mn}_3\text{Sn}$  configuration in Fig. 2 is  $P^{1,1,1}6_3^{3-1}/m^1m^m c^m (C_{3v}^{\text{II}})$ , as shown in Fig. 3.

## B. Coirreps of spin space groups

Since the magnetic translation group  $\mathcal{T}_0 \equiv \{\mathcal{O}_\alpha \in \mathcal{G}_0 | U_\alpha = E, R_\alpha = E\} = \{\{E||E|\lambda\mathbf{t}_1 + \mu\mathbf{t}_2 + \nu\mathbf{t}_3\} | \lambda, \mu, \nu \in \mathbb{Z}\}$  is a normal subgroup of  $\mathcal{G}$  ( $\mathbf{t}_{i=1,2,3}$  are the magnetic primitive lattice vectors), Bloch's theorem applies and the crystal wave vector  $\mathbf{k}$  is a good quantum number. Thus, coirreps of an SSG are classified by  $k$  vectors. One can use a coirrep of the  $k$ -little group to construct the coirrep of the entire SSG, together with the  $k$ -star states. The little group of  $\mathbf{k}$ , denoted as  $LG(\mathbf{k})$ , is defined as

$$LG(\mathbf{k}) = \{\mathcal{O}_\alpha \in \mathcal{G} | \det(U_\alpha)R_\alpha\mathbf{k} = \mathbf{k} + \mathbf{G}\}, \quad \mathbf{G} = l\mathbf{g}_1 + m\mathbf{g}_2 + n\mathbf{g}_3, \quad l, m, n \in \mathbb{Z}, \quad (4)$$

where  $\mathbf{g}_{i=1,2,3}$  are the magnetic primitive reciprocal lattice vectors (*i.e.*,  $\mathbf{g}_i \cdot \mathbf{t}_j = \delta_{ij}$ ). Hereafter, without specific assignment, the SSG is typically referred to as the little group  $LG(\mathbf{k})$ .

To construct the linear coirreps of an SSG  $\mathcal{G}$ , we need to construct the projective coirreps of the quotient group  $\mathcal{F} = \mathcal{G}/\mathcal{W}$ , where  $\mathcal{W} \equiv \mathcal{T}_0 \times \{E, \bar{E}\}$  and  $\bar{E}$  is a  $2\pi$  rotation in spin space. The group  $\mathcal{G}$  is an extension of  $\mathcal{F}$  by  $\mathcal{W}$ . The quotient group can be expressed in terms of cosets as

$$\mathcal{G}/\mathcal{W} \simeq \{g_i\mathcal{W} / \sim: g_i \in \mathcal{G}, g_i \sim g_i h, h \in \mathcal{W}\}, \quad (5)$$

where the elements of the quotient group (*i.e.*,  $g_i, g_j$ , and  $g_i g_j$  are the coset representatives) satisfy

$$(g_i\mathcal{W})(g_j\mathcal{W}) = (g_i g_j\mathcal{W}), \quad (g_i\mathcal{W})^{-1} = (g_i^{-1}\mathcal{W}), \quad e = (\mathcal{W}). \quad (6)$$

This induces a nontrivial factor system (Appendix A) for the projective representation  $M$  of  $\mathcal{F}$  ( $g_i = \mathcal{O}_\alpha$ ,  $g_j = \mathcal{O}_\beta$ ):

$$M(\mathcal{O}_\alpha)M(\mathcal{O}_\beta) = \omega(\mathcal{O}_\alpha, \mathcal{O}_\beta)M(\mathcal{O}_\alpha\mathcal{O}_\beta), \quad \omega(\mathcal{O}_\alpha, \mathcal{O}_\beta) = \omega_\tau(\mathcal{O}_\alpha, \mathcal{O}_\beta)\omega_s(\mathcal{O}_\alpha, \mathcal{O}_\beta). \quad (7)$$

$$\omega_\tau(\mathcal{O}_\alpha, \mathcal{O}_\beta) = \exp[-i\mathbf{k} \cdot (R_\alpha - \det(U_\alpha))\mathbf{v}_\beta], \quad \omega_s(\mathcal{O}_\alpha, \mathcal{O}_\beta) = \pm 1.$$

The factor  $\omega_\tau$  originates from the nontrivial phase induced by the translation subgroup  $\mathcal{T}_0$  acting on Bloch states. The factor  $\omega_s$  originates from the  $2\pi$  spin rotation group. Once we obtain the complete factor system for  $\mathcal{F}$ , the projective coirreps  $M(\mathcal{O}_\alpha)$  of the quotient group  $\mathcal{F}$  can be systematically constructed (Sec. III C 2), from which the double-valued linear representations of the full SSG  $\mathcal{G}$  can be obtained [34].

Since the SSG  $\mathbf{k}$ -little group usually contains anti-unitary operations, we can decompose it as  $LG(\mathbf{k}) = \mathcal{L} + A\mathcal{L}$ , where  $\mathcal{L}$  is the unitary subgroup and  $A$  is an anti-unitary element. The projective corepresentation (corep) is constructed

from an irrep ( $\Delta_a$ ) of the unitary subgroup  $\mathcal{L}$  and its conjugate irrep ( $\Delta_a^*$ ). Whether a projective corep is irreducible is determined by a criterion that is independent of the factor gauge [35, 36]:

$$\frac{1}{|\mathcal{L}|} \sum_{\mathcal{O} \in \mathcal{L}} \frac{1}{2} \left\{ |\text{Tr}[M(\mathcal{O})]|^2 + \text{Tr}[M(A\mathcal{O})M^*(A\mathcal{O})] \right\} = 1. \quad (8)$$

If the projective corep satisfies the condition in Eq. (8), then it is irreducible, being a projective coirrep. These projective coirreps can be classified into three cases by the torsion defined as

$$R = \frac{1}{|\mathcal{L}|} \sum_{\mathcal{O} \in \mathcal{L}} |\chi(\mathcal{O})|^2 = \begin{cases} 1, & \text{real,} & \text{case (a), labeled as } \Delta_a; \\ 2, & \text{complex,} & \text{case (b), labeled as } \Delta_a \Delta_b; \\ 4, & \text{quaternionic, case (c), labeled as } \Delta_a \Delta_a. \end{cases} \quad (9)$$

In case (a), the projective coirrep is formed by a single projective irrep  $\Delta_a$  of  $\mathcal{L}$ , being  $\Delta_a$  coirrep. In case (b), the projective coirrep is formed by the sum of two distinct projective irreps that constitute a complex-conjugate pair ( $\Delta_b = \Delta_a^*$ ), being  $\Delta_a \Delta_b$  coirrep. In case (c), the projective coirrep is formed by the sum of two identical copies ( $\Delta_a = \Delta_a^*$ ), being  $\Delta_a \Delta_a$  coirrep.

### C. Traces of matrix presentations of SSG operations

A unitary operation acting on a spinor-valued function in real space is expressed as  $\mathcal{O}f_\sigma(\mathbf{r}) = \sum_{\sigma'} Q_{\sigma\sigma'} f_{\sigma'}(\{R|\mathbf{v}\}^{-1}\mathbf{r}) = \sum_{\sigma'} Q_{\sigma\sigma'} f_{\sigma'}(R^{-1}\mathbf{r} - R^{-1}\mathbf{v})$ , where  $Q$  is the SU(2) matrix of  $U$ . The matrix presentations (MPs),  $O_i^{mn}$ , can be obtained in the basis of the wavefunctions (WFs)  $|\psi_{n\mathbf{k}}\rangle$  as  $O_\alpha^{mn} = \langle \psi_{m\mathbf{k}} | \mathcal{O}_\alpha | \psi_{n\mathbf{k}} \rangle$ . The traces of the obtained MPs are essential for determining the corresponding irreps of  $LG(\mathbf{k})$  and are defined as

$$\text{Tr}[\mathcal{O}_\alpha] = \sum_n O_\alpha^{nn} \text{ with } O_\alpha^{nn} = \langle \psi_{n\mathbf{k}} | \mathcal{O}_\alpha | \psi_{n\mathbf{k}} \rangle, \quad \mathcal{O}_\alpha \in LG(\mathbf{k}). \quad (10)$$

#### 1. Plane-wave basis

In the plane-wave basis, the spinor WFs are expanded in plane waves as

$$\psi_{n\mathbf{k}}(\mathbf{r}) = \begin{pmatrix} \psi_{n\mathbf{k}\uparrow}(\mathbf{r}) \\ \psi_{n\mathbf{k}\downarrow}(\mathbf{r}) \end{pmatrix} = \sum_j \begin{pmatrix} C_{\uparrow j}^{n\mathbf{k}} \\ C_{\downarrow j}^{n\mathbf{k}} \end{pmatrix} e^{i(\mathbf{k}+\mathbf{G}_j)\cdot\mathbf{r}} = \sum_{j, \zeta \in \{\uparrow, \downarrow\}} C_{\zeta j}^{n\mathbf{k}} e^{i(\mathbf{k}+\mathbf{G}_j)\cdot\mathbf{r}} |\zeta\rangle \text{ with } \langle \mathbf{k} + \mathbf{G}_i | \mathbf{k} + \mathbf{G}_j \rangle = \delta_{ij} \quad (11)$$

The coefficients ( $C_{\zeta j}^{n\mathbf{k}}$ ) are obtained from *ab initio* calculations and are output by DFT packages (*e.g.* VASP and QE). The action of SSG operations on the WFs is derived as

$$\begin{aligned} \mathcal{O}_\alpha \psi_{n\mathbf{k}}(\mathbf{r}) &= \sum_j e^{i(\mathbf{k}+\mathbf{G}_j)\cdot(R_\alpha^{-1}\mathbf{r} - R_\alpha^{-1}\mathbf{v}_\alpha)} Q_\alpha \begin{pmatrix} C_{\uparrow j}^{n\mathbf{k}} \\ C_{\downarrow j}^{n\mathbf{k}} \end{pmatrix} \\ &= \sum_{j\zeta\zeta'} e^{iR_\alpha(\mathbf{k}+\mathbf{G}_j)\cdot(\mathbf{r}-\mathbf{v}_\alpha)} Q_{\alpha,\zeta\zeta'} C_{\zeta'j}^{n\mathbf{k}} |\zeta\rangle \\ &= \sum_{j\zeta\zeta'} e^{i(\mathbf{k}+\mathbf{G}_{j'})\cdot(\mathbf{r}-\mathbf{v}_\alpha)} Q_{\alpha,\zeta\zeta'} C_{\zeta'j}^{n\mathbf{k}} |\zeta\rangle, \text{ with } \mathbf{k} + \mathbf{G}_{j'} \equiv R_\alpha(\mathbf{k} + \mathbf{G}_j) \\ &= e^{-i\mathbf{k}\cdot\mathbf{v}_\alpha} \sum_{j\zeta\zeta'} e^{-i\mathbf{G}_{j'}\cdot\mathbf{v}_\alpha} e^{i(\mathbf{k}+\mathbf{G}_{j'})\cdot\mathbf{r}} Q_{\alpha,\zeta\zeta'} C_{\zeta'j}^{n\mathbf{k}} |\zeta\rangle \text{ with } \mathbf{G}_{j'} \equiv R_\alpha(\mathbf{k} + \mathbf{G}_j) - \mathbf{k}. \end{aligned} \quad (12)$$

Then, Eq. (10) can be written as

$$\langle \psi_{n\mathbf{k}} | \mathcal{O}_\alpha | \psi_{n\mathbf{k}} \rangle = e^{-i\mathbf{k}\cdot\mathbf{v}_\alpha} \sum_{j\zeta\zeta'} C_{\zeta j}^{*n\mathbf{k}} C_{\zeta'j}^{n\mathbf{k}} e^{-i\mathbf{G}_{j'}\cdot\mathbf{v}_\alpha} Q_{\alpha,\zeta\zeta'}, \text{ with } \mathbf{G}_{j'} \equiv R_\alpha(\mathbf{k} + \mathbf{G}_j) - \mathbf{k}. \quad (13)$$

## 2. Localized Wannier basis

In a tight-binding (TB) Hamiltonian, the spinor WFs are expanded in the basis of exponentially localized orthogonal orbitals:  $|\mathbf{0}, \mu a \sigma\rangle \equiv \phi_{a\sigma}^\mu(\mathbf{r}) \equiv \phi_a(\mathbf{r} - \tau_\mu) |\sigma\rangle$  and  $|\mathbf{L}_j, \mu a \sigma\rangle \equiv \phi_a(\mathbf{r} - \mathbf{L}_j - \tau_\mu) |\sigma\rangle$ , where  $\mu$  labels the atoms,  $a$  labels the orbitals,  $\sigma$  labels the spins,  $\mathbf{L}_j$  labels the lattice vectors in 3D crystals, and  $\tau_\mu$  labels the positions of atoms in the home unit cell. At a given  $k$  point, the WFs are given as

$$\begin{aligned} \psi_{n\mathbf{k}}(\mathbf{r}) &= \begin{pmatrix} \psi_{n\mathbf{k}\uparrow}(\mathbf{r}) \\ \psi_{n\mathbf{k}\downarrow}(\mathbf{r}) \end{pmatrix} = \sum_{\mu a} \begin{pmatrix} C_{\mu a \uparrow}^{n\mathbf{k}} \phi_{a\mathbf{k}\uparrow}^\mu(\mathbf{r}) \\ C_{\mu a \downarrow}^{n\mathbf{k}} \phi_{a\mathbf{k}\downarrow}^\mu(\mathbf{r}) \end{pmatrix} = \sum_{\mu a, \sigma=\{\uparrow, \downarrow\}} C_{\mu a \sigma}^{n\mathbf{k}} \phi_{a\mathbf{k}\sigma}^\mu(\mathbf{r}), \text{ where } n \text{ is a band index,} \\ \phi_{a\mathbf{k}\sigma}^\mu(\mathbf{r}) &= \phi_{a\mathbf{k}}^\mu(\mathbf{r}) |\sigma\rangle = \sum_j \phi_a(\mathbf{r} - \tau_\mu - \mathbf{L}_j) e^{i\mathbf{k} \cdot (\mathbf{L}_j + \tau_\mu)} |\sigma\rangle, \left\langle \phi_{b\mathbf{k}\sigma'}^{\mu'} | \phi_{a\mathbf{k}\sigma}^\mu \right\rangle = \delta_{\mu\mu'} \delta_{ab} \delta_{\sigma\sigma'}. \end{aligned} \quad (14)$$

The states  $\phi_{a\mathbf{k}\sigma}^\mu(\mathbf{r})$  are the Fourier transforms of the local orbitals  $\phi_{a\sigma}^\mu(\mathbf{r})$ , as shown in Eq. (14). The coefficients are obtained as eigenvectors of the TB Hamiltonian  $H_{\mu'b\sigma', \mu a \sigma}(\mathbf{k}) = \sum_j e^{i\mathbf{k} \cdot (\mathbf{L}_j + \tau_\mu - \tau_{\mu'})} \langle \mathbf{0}, \mu' b \sigma' | \hat{H} | \mathbf{L}_j, \mu a \sigma \rangle$ . The action of rotational symmetries  $R_\alpha$  on the local orbitals  $\phi_{a\sigma}(\mathbf{r})$  at the  $\mu$  site is given by

$$\widehat{R_\alpha} \phi_{a\sigma}(\mathbf{r}) \equiv R_\alpha \phi_{a\sigma}(\mathbf{r}) = \sum_b \phi_{b\sigma}(\mathbf{r}) D_{ba}^{\alpha, \mu}. \quad (15)$$

These  $D$ -matrices are explicitly given in Table A.3 of Ref. [25]. In the basis of real spherical harmonic functions with different total angular momenta (integer  $l$ ), these  $D$ -matrices are real.

The action of the SSG operation  $\mathcal{O}_\alpha$  on the states  $\psi_{n\mathbf{k}}(\mathbf{r})$  is given by

$$\begin{aligned} &\mathcal{O}_\alpha \psi_{n\mathbf{k}}(\mathbf{r}) \\ &= \sum_{a\mu} Q_\alpha \begin{pmatrix} C_{\mu a \uparrow}^{n\mathbf{k}} \phi_{a\mathbf{k}\uparrow}^\mu(R_\alpha^{-1}\mathbf{r} - R_\alpha^{-1}\mathbf{v}_\alpha) \\ C_{\mu a \downarrow}^{n\mathbf{k}} \phi_{a\mathbf{k}\downarrow}^\mu(R_\alpha^{-1}\mathbf{r} - R_\alpha^{-1}\mathbf{v}_\alpha) \end{pmatrix} \\ &= \sum_{a\mu\zeta\zeta'} Q_{\alpha, \zeta\zeta'} C_{\mu a \zeta'}^{n\mathbf{k}} \phi_{a\zeta'}(R_\alpha^{-1}\mathbf{r} - R_\alpha^{-1}\mathbf{v}_\alpha - \tau_\mu - \mathbf{L}_j) e^{i\mathbf{k} \cdot (\mathbf{L}_j + \tau_\mu)} |\zeta\rangle \\ &= \sum_{a\mu\zeta\zeta'} Q_{\alpha, \zeta\zeta'} C_{\mu a \zeta'}^{n\mathbf{k}} \phi_{a\zeta'}(R_\alpha^{-1}[\mathbf{r} - \mathbf{v}_\alpha - R_\alpha \tau_\mu - R_\alpha \mathbf{L}_j]) e^{i\mathbf{k} \cdot (\mathbf{L}_j + \tau_\mu)} |\zeta\rangle \\ &= \sum_{a\mu\zeta\zeta'} Q_{\alpha, \zeta\zeta'} C_{\mu a \zeta'}^{n\mathbf{k}} \widehat{R_\alpha} \phi_{a\zeta'}([\mathbf{r} - \mathbf{v}_\alpha - R_\alpha \tau_\mu - R_\alpha \mathbf{L}_j]) e^{iR_\alpha \mathbf{k} \cdot [R_\alpha (\mathbf{L}_j + \tau_\mu)]} |\zeta\rangle \\ &= e^{-i(R_\alpha \mathbf{k} \cdot \mathbf{v}_\alpha)} \sum_{a\mu\zeta\zeta'} Q_{\alpha, \zeta\zeta'} C_{\mu a \zeta'}^{n\mathbf{k}} \widehat{R_\alpha} \phi_{a\zeta'}([\mathbf{r} - (\mathbf{v}_\alpha + R_\alpha \tau_\mu) - R_\alpha \mathbf{L}_j]) e^{iR_\alpha \mathbf{k} \cdot [R_\alpha \mathbf{L}_j + (R_\alpha \tau_\mu) + \mathbf{v}_\alpha]} |\zeta\rangle \\ &= e^{-i(R_\alpha \mathbf{k} \cdot \mathbf{v}_\alpha)} \sum_{a\mu\zeta\zeta'} Q_{\alpha, \zeta\zeta'} C_{\mu a \zeta'}^{n\mathbf{k}} \widehat{R_\alpha} \phi_{a\zeta'}(\mathbf{r} - (\tau_{\mu'} + \mathbf{L}_0^i) - R_\alpha \mathbf{L}_j) e^{iR_\alpha \mathbf{k} \cdot [R_\alpha \mathbf{L}_j + (\tau_{\mu'} + \mathbf{L}_0^i)]} |\zeta\rangle \text{ using } \mathbf{v}_\alpha + R_\alpha \tau_\mu = \mathbf{L}_0^i + \tau_{\mu'} \\ &= e^{-i(R_\alpha \mathbf{k} \cdot \mathbf{v}_\alpha)} \sum_{a\mu\zeta\zeta'} Q_{\alpha, \zeta\zeta'} C_{\mu a \zeta'}^{n\mathbf{k}} \widehat{R_\alpha} \phi_{a\zeta'}(\mathbf{r} - \tau_{\mu'} - \mathbf{L}_{j'}) e^{iR_\alpha \mathbf{k} \cdot (\mathbf{L}_{j'} + \tau_{\mu'})} |\zeta\rangle \text{ with } \mathbf{L}_{j'} = \mathbf{L}_0^i + R_\alpha \mathbf{L}_j \\ &= e^{-i(R_\alpha \mathbf{k} \cdot \mathbf{v}_\alpha)} \sum_{ab\mu\zeta\zeta'} Q_{\alpha, \zeta\zeta'} C_{\mu a \zeta'}^{n\mathbf{k}} D_{ba}^{\alpha, \mu} \phi_{b, R_\alpha \mathbf{k}\zeta'}^{\mu'}(\mathbf{r}) |\zeta\rangle \text{ with } \widehat{R_\alpha} \phi_{a\sigma}(\mathbf{r}) \equiv \sum_b \phi_{b\sigma}(\mathbf{r}) D_{ba}^{\alpha, \mu}. \end{aligned} \quad (16)$$

Thus, Eq. (10) can be written as

$$\langle \psi_{n\mathbf{k}} | \mathcal{O}_\alpha | \psi_{n\mathbf{k}} \rangle = e^{-i(R_\alpha \mathbf{k} \cdot \mathbf{v}_\alpha)} \sum_{ab\mu\zeta\zeta'} e^{i(R_\alpha \mathbf{k} - \mathbf{k}) \cdot \tau_{\mu'}} C_{\mu' b \zeta'}^{n\mathbf{k}*} C_{\mu a \zeta'}^{n\mathbf{k}} D_{ba}^{\alpha, \mu} Q_{\alpha, \zeta\zeta'}, \text{ with } \mathbf{v}_\alpha + R_\alpha \tau_\mu = \mathbf{L}_0^i + \tau_{\mu'}. \quad (17)$$

In matrix form,

$$\begin{aligned} \langle \psi_{n\mathbf{k}} | \mathcal{O}_\alpha | \psi_{n\mathbf{k}} \rangle &= e^{-i(R_\alpha \mathbf{k} \cdot \mathbf{v}_\alpha)} \left[ \overline{C(\mathbf{k})^\dagger} [V(R_\alpha \mathbf{k} - \mathbf{k}) \otimes \sigma_0] (D^\alpha \otimes Q_\alpha) C(\mathbf{k}) \right]_{nn}, \\ \text{with } \overline{V(\mathbf{k})}_{\mu' b, \mu a} &= e^{i\mathbf{k} \cdot \tau_\mu} \delta_{\mu\mu'} \delta_{ab}, \quad \overline{C(\mathbf{k})}_{\mu a \zeta, n} = C_{\mu a \zeta}^{n\mathbf{k}}, \quad \overline{D}_{\mu' b, \mu a}^\alpha = \begin{cases} D_{ba}^{\alpha, \mu}, & \text{if } \mathbf{v}_\alpha + R_\alpha \tau_\mu = \mathbf{L}_0^i + \tau_{\mu'}; \\ 0, & \text{otherwise.} \end{cases} \end{aligned} \quad (18)$$

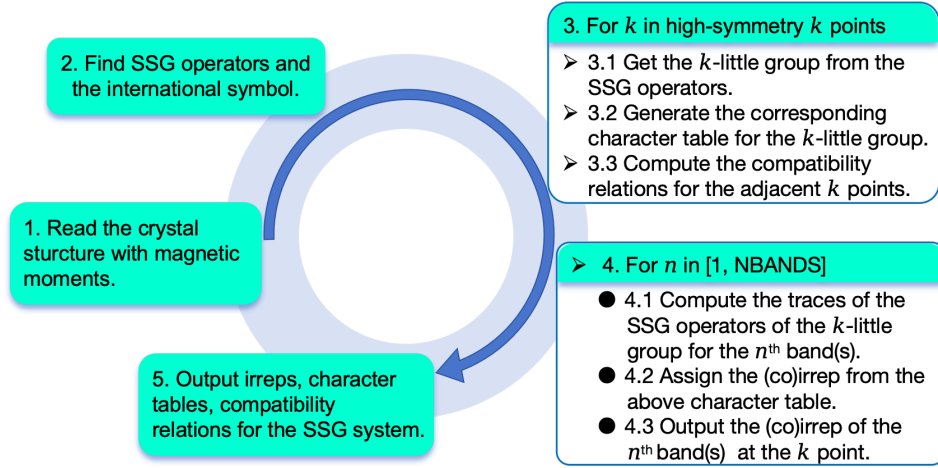


Figure 1: Workflow of IRSSG for spin space groups.

Based on the above derivations, the code has been extended to work with the TB Hamiltonians. Thus, it works for any DFT code that has an interface to Wannier90, *e.g.* VASP, Wien2k [37, 38] and OpenMX [39–41]. To run IRSSG, users must provide two input files: `case_hr.dat` and `tbbox.in`. The file `case_hr.dat` contains the TB parameters and can be generated by Wannier90 [30, 31, 42–44], by users from a toy TB model, or from the Slater-Koster method [45] or by discretization of a  $k \cdot p$  model onto a lattice [46]. The other file, `tbbox.in`, is the master input file for IRSSG and should be consistent with the TB parameters in `case_hr.dat`. An example `tbbox.in` file for  $\text{Mn}_3\text{Sn}$  with a type-II configuration is provided in Appendix B.

Table II: Brief summary of key files.

File	Description	Input
<code>poscar_io.py</code>	Reading POSCAR with magnetic moments.	<i>e.g.</i> POSCAR
<code>find_ssg_operation.py</code>	Finding all operations in $\mathcal{G}_0$ .	
<code>get_ssg_number.py</code>	Obtaining the SSG number.	
<code>get_ssg_symbol.py</code>	Obtaining the SSG international symbol.	
<code>wave_data.f90</code>	Reading the coefficients $C_{\zeta j}^{n\mathbf{k}}$ .	<i>e.g.</i> WAVECAR
<code>get_ssg.f90</code>	Constructing all SSG operations in $\mathcal{G}$ [Eq. (2)].	
<code>kgroup.f90</code>	Determining the $k$ -little groups.	
<code>linear_rep.f90</code>	Constructing character tables at high-symmetry $k$ points	
<code>chrct.f90</code>	Computing the traces [Eq. (13)] and determining the coirreps.	

### III. IMPLEMENTATIONS AND FEATURES

In this section, we focus on the implementation details of the IRSSG software package and introduce the major features of its component framework. IRSSG is developed to determine coirreps of magnetic energy bands for magnetic compounds from DFT calculations (taking VASP as an example in the main text). The package first identifies all SSG operations and determines the SSG international symbol. It then generates the SSG character tables of the little groups at the  $k$  points. Finally, it computes the traces of matrix presentations of SSG operations and assigns the coirrep labels to magnetic energy bands. The main workflow is shown in Fig. 1, and a brief summary of the key files is given in Table II.

#### A. Reading the structure and magnetic moments

The function `read_poscar` in `poscar_io.py` reads the magnetic crystal structure, including lattice vectors, atomic positions, and magnetic moments. The input is a modified POSCAR file, in which magnetic moments in Cartesian



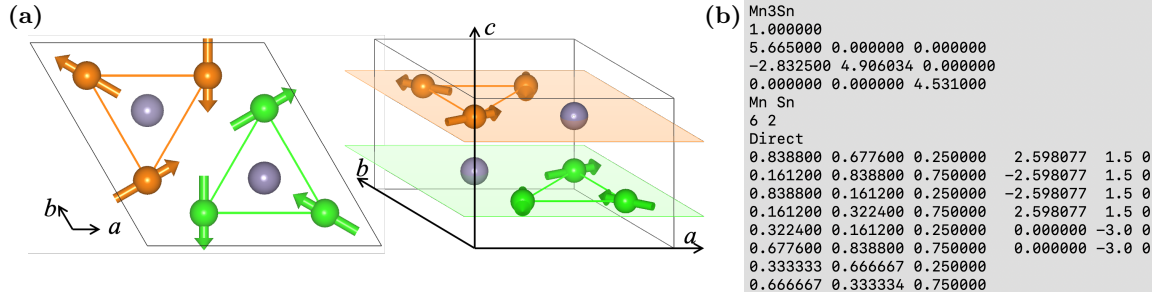


Figure 2: (a) Magnetic crystal structure of Mn<sub>3</sub>Sn with coplanar configuration. (b) The modified POSCAR.

coordinates should follow the fractional coordinates of the atoms. A 5-tuple variable ‘cell’ as defined in Table III is obtained. For instance, the modified POSCAR file of Mn<sub>3</sub>Sn with a type-II configuration is shown in Fig. 2(b).

### B. Finding SSG operations and international symbol

The program IRSSG first determines the SSG magnetic configuration type (I: collinear; II: coplanar; III: noncoplanar). Then, it finds the SSG operations of the subgroup  $\mathcal{G}_0$ . Intuitively, all SSG elements of  $\mathcal{G}_0$  must be contained in the direct product of the moment-part group  $\mathcal{A}$  and the atomic-part group  $\mathcal{B}$  (*i.e.*,  $\mathcal{G}_0 \leq \mathcal{A} \times \mathcal{B}$ ). The moment-part group  $\mathcal{A}$  is an NPG determined solely by the magnetic moments. The atomic space group  $\mathcal{B}$  is a CSG obtained by neglecting magnetic moments. All SSG operations are identified by `find_ssg_operation.py` using the `spglib` [47] and `pymatgen` [48] packages, and a dictionary variable “ssg\_ops” is generated. Additionally, a binary file ‘ssg.data’ is generated, which includes all operations of the full SSG  $\mathcal{G}$ . This file is required for constructing character tables and computing band representations. Once ‘ssg.data’ is prepared with the operations of a CSG or a MSG (as a specific SSG case), IRSSG works for them also.

Then, based on all SSG operations, the SSG number and international symbol are determined by `get_ssg_number.py` and `get_ssg_symbol.py`, respectively. Since the spin space and lattice space are independent, the redefined spin-space coordinates ( $x', y', z'$ ) are output, depending on the spin configuration provided as input. For type-I SSGs, the redefined  $z'$  axis is chosen to align with the spin direction. For type-II SSGs, the  $x'y'$  plane is defined by the spin plane. For type-III SSGs, the  $x'y'z'$  axes are redefined following the standard NPG convention. Under the redefined coordinates, the spin space rotation becomes  $U_\alpha = \zeta_\alpha \oplus I_1$  for type-I and  $U_\alpha = I_2 \oplus \zeta_\alpha$  for type-II. Here,  $I_n$  is the  $n$ -dimensional identity,  $\zeta_\alpha = \pm 1$ , and  $\zeta_\alpha$  is a  $2 \times 2$   $O(2)$  matrix. A screenshot of ‘ssg.out’ for Mn<sub>3</sub>Sn with a coplanar configuration is shown in Fig. 3.

### C. Character tables at high-symmetry $k$ points

We construct the character tables of the coirreps of the  $k$ -little groups  $LG(\mathbf{k})$  at all  $k$  points.

Table III: Structure of the tuple variable “cell” obtained by the function `read_poscar` is given below ( $N$  is the total number of atoms).

Index	Type	Description
0	<code>numpy.ndarray[(3,3), float]</code>	lattice vectors ( $\mathbf{t}_1, \mathbf{t}_2, \mathbf{t}_3$ ) of the magnetic crystal structure
1	<code>numpy.ndarray[(N,3), float]</code>	fractional coordinates of atoms ( $f_1\mathbf{t}_1, f_2\mathbf{t}_2, f_3\mathbf{t}_3$ )
2	<code>list[int]</code>	species indices of atoms
3	<code>list[str]</code>	element symbols of atoms
4	<code>numpy.ndarray[(N,3), float]</code>	magnetic moments of atoms in Cartesian coordinates

```

The SSG number: 194.1.6.1.P
The SSG label: P^{1,1,1} 6_3^{3^{\{-1\}}} / m^1 m^m c^m (C3v^II)
II: Coplanar SSG in the x'y' plane; So: Cs={E,Mz'}
The redefined axes in spin space: (x',y',z')=(x,y,z)D
D = 0.500 -0.866 0.000
    0.866 0.500 0.000
    0.000 0.000 1.000
The SSG G = So x Go
P (spin part of Go): C3v
H (lattice part of Go): P6_3/mmc
=====
Spin space group operations: {U||R|v}
U is given in x'y'z' coordinates, while R is given in the lattice basis of POSCAR.
U= \zeta_{2x2} + I_1 in type II
# Number: 24
{ \zeta_{2x2} || Ri | taui }
# 1 without time-reversal
1.000 0.000 1 0 0 0.000
0.000 1.000 0 1 0 0.000
0 0 1 0.000

```

Figure 3: Screenshot of 'ssg.out'.

### 1. Obtaining the SSG $k$ -little group

The SSG operations are read from 'ssg.data' by `get_ssg.f90`. An SSG operation that leaves  $\mathbf{k}$  invariant up to a reciprocal-lattice vector [Eq. (4)] belongs to the  $k$ -little group; this is implemented in `kgroup.f90`. All related variables are summarized in Table IV in detail.

### 2. Generating the character table of the $k$ -little group

In this part, we use the Hamiltonian method to decompose the regular projective corep to obtain the projective coirreps, and finally obtain the linear coirreps, which are all done in file `linear_rep.f90`. The related variable is listed in Table IV, while `Ncoirrep` and `Ch_table2` are valid only when `aunt=2`.

The factor system  $\omega$  is obtained from Eq. (7). The regular projective corep is then constructed as

$$M_{ij}(\mathcal{O}_\alpha) = \begin{cases} \omega(\mathcal{O}_\alpha, \mathcal{O}_j) \delta_{\mathcal{O}_i, [\mathcal{O}_\alpha \mathcal{O}_j]}, & \mathcal{O}_\alpha \text{ is unitary,} \\ \omega(\mathcal{O}_\alpha, \mathcal{O}_j) \delta_{\mathcal{O}_i, [\mathcal{O}_\alpha \mathcal{O}_j]} \mathcal{K}, & \mathcal{O}_\alpha \text{ is anti-unitary,} \end{cases}$$

with  $\mathcal{O}_\alpha, \mathcal{O}_i, \mathcal{O}_j, [\mathcal{O}_\alpha \mathcal{O}_j] \in LG(\mathbf{k})$

(19)

where  $\mathcal{K}$  is the complex conjugation.

The regular projective corep is completely reducible and decomposes as the direct sum of all inequivalent projective coirreps,  $M \cong \bigoplus_\rho d_\rho M^{(\rho)}$ , where  $M^{(\rho)}$  is the matrix of projective coirrep  $\rho$ , and  $d_\rho$  is its multiplicity, equal to the dimension divided by the torsion of  $\rho$ . Thus, the projective coirreps are obtained by decomposing the regular projective corep using the Hamiltonian method. The results are written to 'chart.dat'.

Table IV: Brief summary of variables on SSG  $\mathcal{G}$  and the little group  $LG(\mathbf{k})$ .

	Variables	Type	Description
SSG $\mathcal{G}$	<code>num_sym</code>	<code>integer</code>	Total number of operations in SSG $\mathcal{G}$ (i.e., $\mathcal{G}/\mathcal{T}_0$ ).
	<code>Spin_rot(3,3,num_sym)</code>	<code>real</code>	$U_\alpha$ : spin part of operations $\mathcal{O}_\alpha \in \mathcal{G}$ .
	<code>Rot(3,3,num_sym)</code>	<code>integer</code>	$R_\alpha$ : rotation part of operations $\mathcal{O}_\alpha \in \mathcal{G}$ .
	<code>Tau(3,num_sym)</code>	<code>real</code>	$v_\alpha$ : translation part of operations $\mathcal{O}_\alpha \in \mathcal{G}$ .
$LG(\mathbf{k})$	<code>NumLG</code>	<code>integer</code>	Total number of SSG operations in the little group $LG(\mathbf{k})$ .
	<code>litt_group(:)</code>	<code>integer</code>	Indices of SSG operations belonging to $LG(\mathbf{k})$ .
	<code>aunt</code>	<code>integer</code>	Flag for (anti-)unitarity of $LG(\mathbf{k})$ , 1: unitary, 2: anti-unitary.
	<code>Nirrep</code>	<code>integer</code>	Number of irreps of the unitary group of $LG(\mathbf{k})$ .
	<code>Ch_table1(Nirrep,NumLG/aunt)</code>	<code>complex</code>	Characters of the irreps for the unitary subgroup of $LG(\mathbf{k})$ .
	<code>Ncoirrep</code>	<code>integer</code>	Total number of coirreps of $LG(\mathbf{k})$ .
	<code>Ch_table2(Ncoirrep,NumLG/aunt)</code>	<code>complex</code>	Characters of the unitary operations in the coirreps of $LG(\mathbf{k})$ .



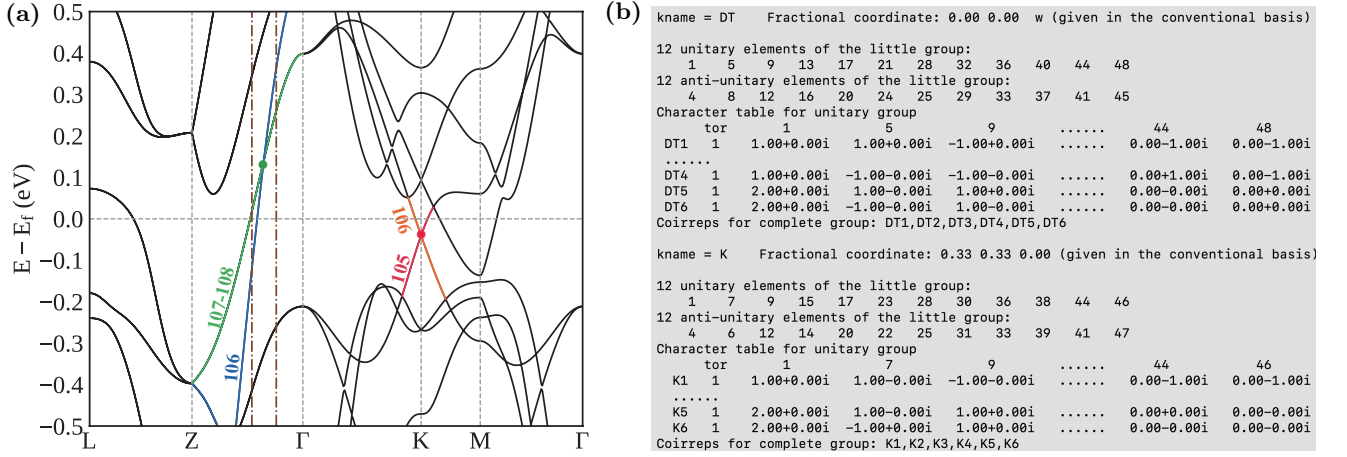


Figure 4: (a) Magnetic energy bands of Mn<sub>3</sub>Sn with a type-II configuration. (b) Screenshot of ‘chart.dat’.

### 3. Obtaining compatibility relations

Due to subgroup relations between the SSG little groups of adjacent  $k$  points, the compatibility relations are generated accordingly. They are written to ‘chart.dat’ as well.

## D. Computing the coirreps of magnetic energy bands

For each  $k$  point, we obtain the coirreps of all magnetic energy bands.

### 1. Computing the traces of the SSG operations in the $k$ -little group

The coefficients  $C_{\xi j}^{nk}$  in Eq. (11) are stored in the WAVECAR generated by VASP and wfc.dat generated by QE. All coefficients are read by wave\_data.f90 and stored in the complex variables coeffa ( $C_{\uparrow j}^{nk}$ ) and coeffb ( $C_{\downarrow j}^{nk}$ ). To compute traces only, one can use the plane-wave wavefunctions directly. The characters of SSG elements of  $LG(\mathbf{k})$  are then computed using Eq. (13) for degenerate bands. In addition, IRSSG can compute the traces of SSG operations in the orthogonal localized Wannier basis via Eq. (17).

### 2. Assigning coirreps to magnetic energy bands

By comparing the obtained traces with the traces of the character tables, one can easily assign the coirreps, which is done in chrct.f90.

## E. Outputting coirreps, character tables, and compatibility relations for the SSG system

The band characters and their coirreps are presented in the file ‘irssg.out’. Fig. 5 shows excerpts of this file for Mn<sub>3</sub>Sn with a type-II configuration. This file first lists all operations of  $\mathcal{G}/\mathcal{T}_0$ , each assigned an operation index. The character tables are output in the ‘chart.dat’ file along with compatibility relations. This file presents the character tables for irreps of the unitary subgroups of  $LG(\mathbf{k})$  at all  $k$  points with distinct labels, and provides the compatibility relations between adjacent  $k$  points. Fig. 4(b) shows a screenshot of the ‘chart.dat’ file for Mn<sub>3</sub>Sn with a type-II configuration.

#### IV. CAPABILITIES OF THE PROGRAM

Determining the representations of computed electronic bands is crucial for studying phenomena such as band crossings, high degeneracies, and  $k \cdot p$  models and related effects. While tools such as **Phonopy** and **MOM2MSG** [49] can identify the CSG or MSG of materials, there has been no broadly available utility to identify the SSG of materials. For a given magnetic material, **IRSSG** determines the SSG operations and directly outputs the SSG number and international symbol via the command ‘**irssg -ssg**’. Although the complete character tables for CSGs and MSGs are available in the literature [50–52], the character tables of SSGs are not yet broadly accessible. Our program **IRSSG** can also obtain the  $k$ -little group and generate character tables for SSGs. In addition, it can determine the coirreps of magnetic energy bands based on DFT calculations or Wannier functions. Furthermore, similar to **POS2MSG** [32], we developed an auxiliary tool, **POS2SSG**, to generate highest-symmetry magnetic configurations by assigning magnetic moments to magnetic atoms, thereby producing structures with specific SSG numbers specified by the user.

#### V. INSTALLATION AND USAGE OF IRSSG

**IRSSG** is an open-source package released on GitHub under the GNU Lesser General Public License, <https://www.gnu.org/licenses/lgpl-3.0.html>. It can be downloaded directly from the public code archive: <https://github.com/zjwang11/IRSSG>. To build and install **IRSSG**, Python 3.8–3.13 is required. The executable **irssg** and its dependencies are automatically downloaded and installed, and the coirreps of the  $m$ th- $n$ th magnetic energy bands can be obtained by typing:

```
$ pip install irssg
$ irssg -ssg > ssg.out
$ irssg [ -nb $m $n ] > irssg.out
```

Here, we take coplanar  $\text{Mn}_3\text{Sn}$  as an example to illustrate the procedure. The magnetic configuration [53] is shown in Fig. 2(a). The corresponding modified **POSCAR** is shown in Fig. 2(b). Then one can run the command ‘**irssg -ssg > ssg.out**’, which generates the ‘ssg.out’ (only the modified **POSCAR** is required as input), as shown in Fig. 3. From this output, one can find that the SSG international symbol for the  $\text{Mn}_3\text{Sn}$  configuration is  $P^{1,1,1}6_3^{3-1}/m^1m^m c^m(C_{3v}^{\text{II}})$  with SSG number 194.1.6.1.P. In addition, the redefined coordinates in spin space, the spin part group  $\mathcal{P}$  and the lattice part group  $\mathcal{H}$  of the SSG are also presented. The elements ( $\{U||R|\mathbf{v}\}$ ) of the SSG are generated.

We first perform the self-consistent and band-structure DFT calculations for the magnetic configurations (*e.g.* setting ‘**NONCOLLINEAR=.TRUE.; LSORBIT=.FALSE.**’ in **INCAR** for VASP). The wavefunctions must be output in the DFT calculation. The noncollinear band structure for  $\text{Mn}_3\text{Sn}$  is obtained in Fig. 4(a). We can find that there might be two ‘crossing’ points around the Fermi level, which need to be confirmed by the SSG coirreps. Then one can use the command ‘**irssg -nb 103 108 > irssg.out**’ to obtain the SSG coirreps of 103-108 -th bands, with the results written to ‘irssg.out’. The character tables (including compatibility relations) for all  $k$  points are generated in ‘chart.dat’, whose screenshot is given in Fig. 4(b). Explicitly, the screenshots of ‘irssg.out’ are given in Fig. 5 for the three  $k$  points (denoted by two brown dash-dot lines in Fig. 4(a) and K), which indicate that the crossing at ZF is a 3-fold crossing point, formed by DT4 (106-th band) and DT6 (107-th and 108-th bands). The Dirac point at K forms a K6 coirrep, indicating that it is a symmetry-enforced, conventional twofold band-degeneracy point [54]. The coirrep matrices of the generators of  $LG(K)$  are  $D(\{E||M_z|0,0,\frac{1}{2}\}) = -\sigma_0$ ,  $D(\{C_{3z}^{-1}||C_{3z}|0,0,0\}) = \frac{1}{2}(\sigma_0 - \sqrt{3}i\sigma_z)$ ,  $D(\{C_{2(\frac{\sqrt{3}}{2},\frac{1}{2},0)}||M_y|0,0,\frac{1}{2}\}) = -i\sigma_x$ , and  $D(\{M_z||P|0,0,0\}) = \sigma_x\mathcal{K}$ . Based on the coirrep matrices of the generators, the  $k \cdot p$  effective model is also obtained for the SSG system via the invariant theory

$$H(k_x, k_y, k_z) = \begin{pmatrix} 0 & b_1 k_- + c_2 k_+^2 \\ b_1 k_+ + c_2 k_-^2 & 0 \end{pmatrix} + [a_1 + c_1(k_x^2 + k_y^2) + c_3 k_z^2]\sigma_0 \quad (20)$$

where  $k_{\pm} = k_x \pm ik_y$ , and the  $k \cdot p$  parameters are  $a_1 = 9.0882\text{eV}$ ,  $b_1 = 1.0768\text{eV} \cdot \text{\AA}$ ,  $c_1 = 1.9892\text{eV} \cdot \text{\AA}^2$ ,  $c_2 = 1.3385\text{eV} \cdot \text{\AA}^2$  and  $c_3 = -11.9826\text{eV} \cdot \text{\AA}^2$ . The parameters are obtained by using **VASP2KP** in the DFT band structure directly [55]. One can clearly see that it is a quasi-2D-Dirac point with linear dispersions in the  $xy$  plane, while it is quadratic (and doubly degenerate) in the  $z$  direction. A nontrivial  $\pi$  Berry phase of the circle surrounding it can be obtained.

	bnd	ndg	eigval	1	5	9	...	40	44	48	
(a)	103	1	0.8379E+01	1.00+0.00i	0.75+0.66i	-1.00-0.00i	...	0.00-1.00i	0.66-0.75i	0.00-1.00i	= DT1
	104	2	0.8713E+01	2.00+0.00i	0.75+0.66i	1.00-0.00i	...	0.00+0.00i	-0.00+0.00i	0.00-0.00i	= DT5
	106	1	0.9008E+01	1.00+0.00i	-0.75-0.66i	-1.00+0.00i	...	0.00-1.00i	-0.66+0.75i	0.00-1.00i	= DT4
	107	2	0.9145E+01	2.00+0.00i	-0.75-0.66i	1.00-0.00i	...	0.00+0.00i	0.00-0.00i	0.00-0.00i	= DT6
(b)	103	1	0.8409E+01	1.00+0.00i	0.93+0.37i	-1.00-0.00i	...	0.00-1.00i	0.37-0.93i	0.00-1.00i	= DT1
	104	2	0.8868E+01	2.00+0.00i	0.93+0.37i	1.00-0.00i	...	0.00+0.00i	-0.00+0.00i	0.00-0.00i	= DT5
	106	2	0.9389E+01	2.00+0.00i	-0.93-0.37i	1.00-0.00i	...	0.00-0.00i	0.00+0.00i	0.00+0.00i	= DT6
	108	1	0.9492E+01	1.00+0.00i	-0.93-0.37i	-1.00+0.00i	...	0.00-1.00i	-0.37+0.93i	0.00-1.00i	= DT4
(c)	103	2	0.8861E+01	2.00+0.00i	1.00-0.00i	1.00+0.00i	...	0.00+0.00i	0.00-0.00i	0.00-0.00i	= K5
	105	2	0.9088E+01	2.00+0.00i	-1.00+0.00i	1.00+0.00i	...	0.00+0.00i	0.00+0.00i	0.00-0.00i	= K5
	107	2	0.9221E+01	2.00+0.00i	1.00+0.00i	1.00-0.00i	...	0.00+0.00i	0.00+0.00i	0.00-0.00i	= K5

Figure 5: The band coirreps determined by IRSSG, which are output in ‘irssg.out’. The first three columns give band indices, degeneracies, and energies (without subtracting the Fermi level  $E_F$ ), respectively. Then the band characters of each unitary operation and the band coirreps are given in the following lines. Panels (a)–(c) correspond to the two DT points (two dash-dotted lines in Fig. 4(a)) and the K point.

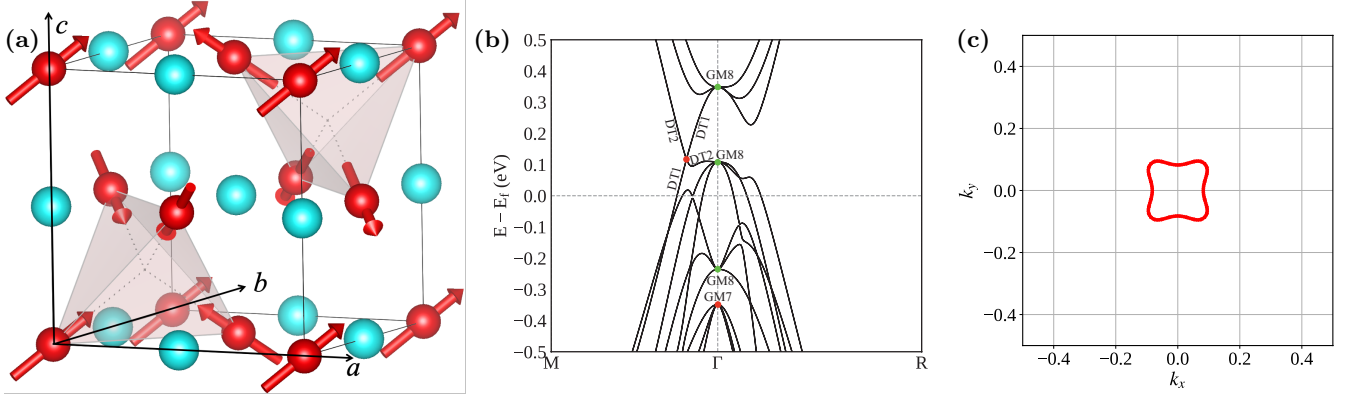


Figure 6: (a) Magnetic crystal structure of NpBi with a type-III configuration, where Np atoms are magnetic. (b) Magnetic energy bands of NpBi. (c) The fourfold nodal line of NpBi in the  $k_z = 0$  plane.

## VI. EXAMPLES

### A. The fourfold nodal lines in NpBi

The noncoplanar magnetic configuration of NpBi [56] is illustrated in Fig. 6(a). Its SSG international symbol  $F^{2,2,2}m^1\bar{3}^3m^m(T_d^{III})$  and SSG number 225.4.6.2 are obtained by IRSSG. After the noncollinear DFT calculations in the absence of SOC, the band structure is obtained along M $\Gamma$ R (Fig. 6(b)) and the wavefunctions (*e.g.* WAVECAR in VASP) are written out as well. By the command ‘irssg -nb 63 86 > irssg.out’, the coirreps are generated for 63-86 -th bands. We find that the crossing along M $\Gamma$  is formed by DT1 and DT2. The crossing is fourfold. In addition, the fourfold crossing is part of the fourfold nodal line in the  $k_z = 0$  plane, as shown in Fig. 6(c). Due to the presence of  $\{C_{3(111)}|C_{3(111)}|0,0,0\}$ , the symmetry-related nodal lines appear in the  $k_x = 0$  and  $k_y = 0$  planes as well. The detailed coirrep analysis shows that the band inversion happens between GM8- and GM7-coirrep bands at  $\Gamma$ , both of which are sixfold. The fourfold nodal lines are actually formed by this sixfold band inversion. All the general bands are doubly degenerate due to the presence of two unitary SSG symmetries at any arbitrary  $k$  point,  $\mathcal{O}_\alpha = \{C_{2x}|E|0, \frac{1}{2}, \frac{1}{2}\}$  and  $\mathcal{O}_\beta = \{C_{2y}|E|\frac{1}{2}, 0, \frac{1}{2}\}$ , with the anti-commutation relation ( $\{Q_\alpha, Q_\beta\} = 0$ ).

### B. The $E_F$ -enforced degenerate point in Eu<sub>3</sub>PbO

The crystal structure of Eu<sub>3</sub>PbO is shown in Fig. 7(a), which is an anti-perovskite structure with Pb at the A site and O at the B site [57]. The noncoplanar magnetic configuration is illustrated in Fig. 7(b), with SSG international symbol  $P^{m,m,m}m^1\bar{3}^3m^m(O_h^{III})$  and SSG number 221.8.6.1 obtained by IRSSG. After the noncollinear calculations in the absence of SOC, the band structure and the wavefunctions are obtained along high-symmetry lines (as shown in Fig. 7(c)). By the command ‘irssg -nb 487 492 > irssg.out’, the coirreps are generated for bands 487 through 492. The total number of electrons is 488 for the compound. We conclude that the crossing along  $\Gamma$ X is formed by DT2 (twofold) and DT5 (fourfold). The detailed analysis shows that the band inversion happens between GM5

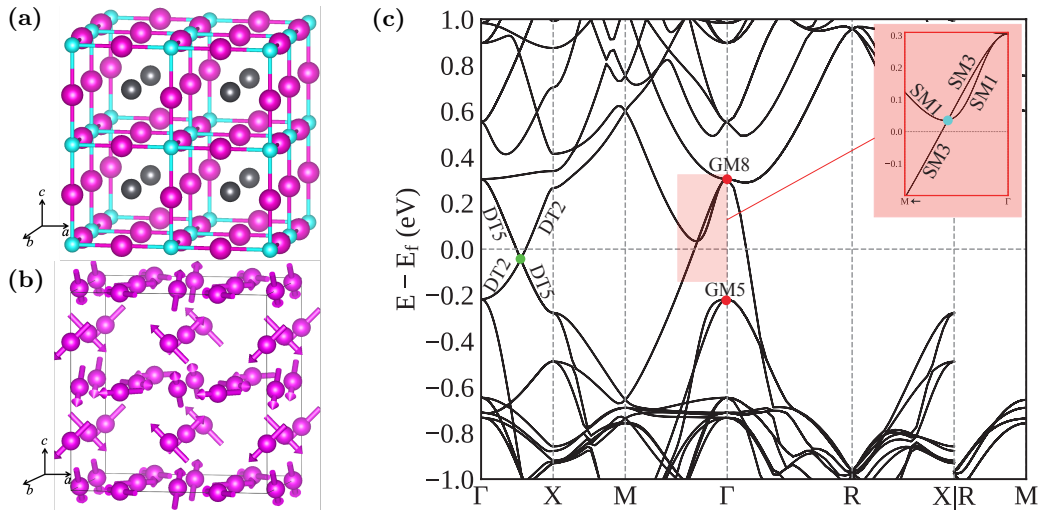


Figure 7: (a) Crystal structure of Eu<sub>3</sub>PbO. (b) Magnetic structure of Eu in Eu<sub>3</sub>PbO. (c) Magnetic energy bands of Eu<sub>3</sub>PbO.

(fourfold) and GM8 (sixfold), resulting in a high-degeneracy point at the Fermi level. The red line is the highest valence band, while the blue line is the lowest conduction band. All the bands are doubly degenerate due to the presence of two unitary SSG symmetries with the anti-commutation relation ( $\{C_{2x}||E|\frac{1}{2}, \frac{1}{2}, 0\}$  and  $\{C_{2y}||E|0, \frac{1}{2}, \frac{1}{2}\}$ ).

## VII. CONCLUSIONS

In summary, we have developed an open-source software package – **IRSSG** – representing the first computational code to determine the coirreps of magnetic states in spin space groups. It first generates the SSG operations, numbers, and international symbols for magnetic crystal structures; second, it constructs character tables for high-symmetry  $k$  points; and finally, it computes the traces of SSG operations and assigns coirreps of the magnetic energy bands obtained from DFT codes. In addition, with a proper ‘sbg.data’, it also works for the 230 CSGs and 1651 MSGs. We further demonstrate how to use it to identify coirreps and high-degeneracy excitations in magnetic materials. This program does not restrict the user to a single DFT program or a single TB Hamiltonian. It works for the DFT codes, such as VASP and Quantum ESPRESSO, as well as any other code that has an interface to Wannier90. The program is very important for advancing research on the study of magnons, altermagnetism, magnetic topology, and novel high-degeneracy excitations in SSG systems.

### Declaration of competing interest

The authors declare that they have no known competing financial interests or personal relationships that could have appeared to influence the work reported in this paper.

**Acknowledgments** We thank Prof. Chen Fang and Dr. Yi Jiang for helpful discussions. This work was supported by the National Key R&D Program of China (Grants No. 2022YFA1403800), National Natural Science Foundation of China (Grants No. 12188101), and the Center for Materials Genome.

- 
- [1] N. A. Benedek and C. J. Fennie, Phys. Rev. Lett. **106**, 107204 (2011), URL <https://link.aps.org/doi/10.1103/PhysRevLett.106.107204>.
  - [2] S. Zhang, Y. Liu, Z. Sun, X. Chen, B. Li, S. L. Moore, S. Liu, Z. Wang, S. E. Rossi, R. Jing, et al., Nature Communications **14**, 6200 (2023), ISSN 2041-1723, URL <https://doi.org/10.1038/s41467-023-41773-x>.
  - [3] G. Yu, J. Ji, Y. Chen, C. Xu, and H. J. Xiang, Phys. Rev. Lett. **134**, 016801 (2025), URL <https://link.aps.org/doi/10.1103/PhysRevLett.134.016801>.
  - [4] E. Galiffi, G. Carini, X. Ni, G. Álvarez Pérez, S. Yves, E. M. Renzi, R. Nolen, S. Wasserroth, M. Wolf, P. Alonso-Gonzalez, et al., Nature Reviews Materials **9**, 9 (2024), ISSN 2058-8437, URL <https://doi.org/10.1038/s41578-023-00620-7>.
  - [5] L. Shu, Y. Xia, B. Li, L. Peng, H. Shao, Z. Wang, Y. Cen, H. Zhu, and H. Zhang, npj Computational Materials **10**, 2 (2024), ISSN 2057-3960, URL <https://doi.org/10.1038/s41524-023-01162-w>.

- [6] Y.-Q. Lin, S.-H. Cao, C.-E. Hu, H.-Y. Geng, and X.-R. Chen, Phys. Rev. B **110**, 075414 (2024), URL <https://link.aps.org/doi/10.1103/PhysRevB.110.075414>.
- [7] H. Zhang, C.-X. Liu, X.-L. Qi, X. Dai, Z. Fang, and S.-C. Zhang, Nature Physics **5**, 438 (2009), ISSN 1745-2481, publisher: Nature Publishing Group, URL <https://www.nature.com/articles/nphys1270>.
- [8] T. H. Hsieh, H. Lin, J. Liu, W. Duan, A. Bansil, and L. Fu, Nature Communications **3**, 982 (2012), ISSN 2041-1723, URL <https://doi.org/10.1038/ncomms1969>.
- [9] L. Elcoro, B. J. Wieder, Z. Song, Y. Xu, B. Bradlyn, and B. A. Bernevig, Nature Communications **12**, 5965 (2021), ISSN 2041-1723, URL <https://doi.org/10.1038/s41467-021-26241-8>.
- [10] J. Yao, R. Zhang, S. Zhang, H. Sheng, Y. Shi, Z. Fang, H. Weng, and Z. Wang, Phys. Rev. B **111**, L041117 (2025), URL <https://link.aps.org/doi/10.1103/PhysRevB.111.L041117>.
- [11] S. Ono, Y. Yanase, and H. Watanabe, Phys. Rev. Res. **1**, 013012 (2019), URL <https://link.aps.org/doi/10.1103/PhysRevResearch.1.013012>.
- [12] S. Ono and K. Shiozaki, Phys. Rev. X **12**, 011021 (2022), URL <https://link.aps.org/doi/10.1103/PhysRevX.12.011021>.
- [13] S. Ono, H. C. Po, and H. Watanabe, Science Advances **6**, eaaz8367 (2020), URL <https://www.science.org/doi/abs/10.1126/sciadv.aaz8367>.
- [14] C. J. Bradley and B. L. Davies, Rev. Mod. Phys. **40**, 359 (1968), URL <https://link.aps.org/doi/10.1103/RevModPhys.40.359>.
- [15] W. F. Brinkman and R. J. Elliott, Proceedings of the Royal Society of London. Series A. Mathematical and Physical Sciences **294**, 343 (1966), URL <https://royalsocietypublishing.org/doi/abs/10.1098/rspa.1966.0211>.
- [16] Z. Xiao, J. Zhao, Y. Li, R. Shindou, and Z.-D. Song, Phys. Rev. X **14**, 031037 (2024), URL <https://link.aps.org/doi/10.1103/PhysRevX.14.031037>.
- [17] X. Chen, J. Ren, Y. Zhu, Y. Yu, A. Zhang, P. Liu, J. Li, Y. Liu, C. Li, and Q. Liu, Phys. Rev. X **14**, 031038 (2024), URL <https://link.aps.org/doi/10.1103/PhysRevX.14.031038>.
- [18] Y. Jiang, Z. Song, T. Zhu, Z. Fang, H. Weng, Z.-X. Liu, J. Yang, and C. Fang, Phys. Rev. X **14**, 031039 (2024), URL <https://link.aps.org/doi/10.1103/PhysRevX.14.031039>.
- [19] A. Corticelli, R. Moessner, and P. A. McClarty, Phys. Rev. B **105**, 064430 (2022), URL <https://link.aps.org/doi/10.1103/PhysRevB.105.064430>.
- [20] X. Chen, Y. Liu, P. Liu, Y. Yu, J. Ren, J. Li, A. Zhang, and Q. Liu, Nature **640**, 349 (2025), ISSN 1476-4687, URL <https://doi.org/10.1038/s41586-025-08715-7>.
- [21] X. Feng and Z. Zhang, Phys. Rev. B **111**, 054520 (2025), URL <https://link.aps.org/doi/10.1103/PhysRevB.111.054520>.
- [22] L. Šmejkal, J. Sinova, and T. Jungwirth, Phys. Rev. X **12**, 031042 (2022), URL <https://link.aps.org/doi/10.1103/PhysRevX.12.031042>.
- [23] L. Šmejkal, J. Sinova, and T. Jungwirth, Phys. Rev. X **12**, 040501 (2022), URL <https://link.aps.org/doi/10.1103/PhysRevX.12.040501>.
- [24] Z. Liu, M. Wei, W. Peng, D. Hou, Y. Gao, and Q. Niu, Phys. Rev. X **15**, 031006 (2025), URL <https://link.aps.org/doi/10.1103/PhysRevX.15.031006>.
- [25] J. Gao, Q. Wu, C. Persson, and Z. Wang, Comput. Phys. Commun. **261**, 107760 (2021), ISSN 0010-4655, code available at <https://github.com/zjwang11/IRVSP>.
- [26] G. Kresse and J. Furthmüller, Phys. Rev. B **54**, 11169 (1996), URL <https://link.aps.org/doi/10.1103/PhysRevB.54.11169>.
- [27] G. Kresse and J. Furthmüller, Computational Materials Science **6**, 15 (1996), ISSN 0927-0256, URL <https://www.sciencedirect.com/science/article/pii/S0927025696000080>.
- [28] P. Giannozzi, S. Baroni, N. Bonini, M. Calandra, R. Car, C. Cavazzoni, D. Ceresoli, G. L. Chiarotti, M. Cococcioni, I. Dabo, et al., Journal of Physics: Condensed Matter **21**, 395502 (2009), URL <https://doi.org/10.1088/0953-8984/21/39/395502>.
- [29] P. Giannozzi, O. Andreussi, T. Brumme, O. Bunau, M. Buongiorno Nardelli, M. Calandra, R. Car, C. Cavazzoni, D. Ceresoli, M. Cococcioni, et al., Journal of Physics: Condensed Matter **29**, 465901 (2017), URL <https://doi.org/10.1088/1361-648X/aa8f79>.
- [30] N. Marzari, A. A. Mostofi, J. R. Yates, I. Souza, and D. Vanderbilt, Rev. Mod. Phys. **84**, 1419 (2012), URL <https://link.aps.org/doi/10.1103/RevModPhys.84.1419>.
- [31] A. A. Mostofi, J. R. Yates, G. Pizzi, Y.-S. Lee, I. Souza, D. Vanderbilt, and N. Marzari, Computer Physics Communications **185**, 2309 (2014), ISSN 0010-4655, URL <https://www.sciencedirect.com/science/article/pii/S001046551400157X>.
- [32] J. Gao, Z. Guo, H. Weng, and Z. Wang, Phys. Rev. B **106**, 035150 (2022), website at [https://tm.iphy.ac.cn/TopMat\\_1651msg.html](https://tm.iphy.ac.cn/TopMat_1651msg.html), URL <https://link.aps.org/doi/10.1103/PhysRevB.106.035150>.
- [33] J. Gao, Y. Qian, H. Jia, Z. Guo, Z. Fang, M. Liu, H. Weng, and Z. Wang, Science Bulletin **67**, 598 (2022), ISSN 2095-9273, website at <https://tm.iphy.ac.cn/UnconvMat.html>, URL <https://www.sciencedirect.com/science/article/pii/S2095927321008045>.
- [34] Z. Song, A. Z. Yang, Y. Jiang, Z. Fang, J. Yang, C. Fang, H. Weng, and Z.-X. Liu, Phys. Rev. B **111**, 134407 (2025), URL <https://link.aps.org/doi/10.1103/PhysRevB.111.134407>.
- [35] Z.-Y. Yang, J. Yang, C. Fang, and Z.-X. Liu, Journal of Physics A: Mathematical and Theoretical **54**, 265202 (2021), URL <https://doi.org/10.1088/1751-8121/abfffc>.
- [36] S. K. Kim, Journal of Mathematical Physics **25**, 2125 (1984), ISSN 0022-2488, URL <https://doi.org/10.1063/1.526419>.
- [37] P. Blaha, K. Schwarz, F. Tran, R. Laskowski, G. K. H. Madsen, and L. D. Marks, The Journal of Chemical Physics **152**,



- 074101 (2020), ISSN 0021-9606, URL <https://doi.org/10.1063/1.5143061>.
- [38] K. Schwarz, P. Blaha, and G. Madsen, Computer Physics Communications **147**, 71 (2002), ISSN 0010-4655, proceedings of the Europhysics Conference on Computational Physics Computational Modeling and Simulation of Complex Systems, URL <https://www.sciencedirect.com/science/article/pii/S0010465502002060>.
  - [39] T. Ozaki and H. Kino, Phys. Rev. B **72**, 045121 (2005), URL <https://link.aps.org/doi/10.1103/PhysRevB.72.045121>.
  - [40] T. Ozaki and H. Kino, Phys. Rev. B **69**, 195113 (2004), URL <https://link.aps.org/doi/10.1103/PhysRevB.69.195113>.
  - [41] T. Ozaki, Phys. Rev. B **67**, 155108 (2003), URL <https://link.aps.org/doi/10.1103/PhysRevB.67.155108>.
  - [42] Q. Wu, S. Zhang, H.-F. Song, M. Troyer, and A. A. Soluyanov, Computer Physics Communications **224**, 405 (2018), ISSN 0010-4655, URL <https://www.sciencedirect.com/science/article/pii/S0010465517303442>.
  - [43] C. Yue, *Symmetrization of wannier tight-binding models (wannhr-symm)*, [https://github.com/quanshengwu/wannier\\_tools/tree/master/utility/wannhr\\_symm](https://github.com/quanshengwu/wannier_tools/tree/master/utility/wannhr_symm) (2018), part of WannierTools; introduced in v2.4.0; accessed 2025-10-20, URL [https://github.com/quanshengwu/wannier\\_tools/tree/master/utility/wannhr\\_symm](https://github.com/quanshengwu/wannier_tools/tree/master/utility/wannhr_symm).
  - [44] D. Gresch, Q. Wu, G. W. Winkler, R. Häuselmann, M. Troyer, and A. A. Soluyanov, Phys. Rev. Mater. **2**, 103805 (2018), URL <https://link.aps.org/doi/10.1103/PhysRevMaterials.2.103805>.
  - [45] J. C. Slater and G. F. Koster, Phys. Rev. **94**, 1498 (1954), URL <https://link.aps.org/doi/10.1103/PhysRev.94.1498>.
  - [46] M. Willatzen and L. C. L. Y. Voon, *The kp method: electronic properties of semiconductors*, vol. 1 (Springer, 2009).
  - [47] A. Togo, K. Shinohara, and I. Tanaka, Science and Technology of Advanced Materials: Methods **4**, 2384822 (2024), URL <https://doi.org/10.1080/27660400.2024.2384822>.
  - [48] S. P. Ong, W. D. Richards, A. Jain, G. Hautier, M. Kocher, S. Cholia, D. Gunter, V. L. Chevrier, K. A. Persson, and G. Ceder, Computational Materials Science **68**, 314 (2013), ISSN 0927-0256, URL <https://www.sciencedirect.com/science/article/pii/S0927025612006295>.
  - [49] Z. Wang, *Mom2ssg*, code available at <https://github.com/zjwang11/TopMat>.
  - [50] M. I. Aroyo, J. M. Perez-Mato, C. Capillas, E. Kroumova, S. Ivantchev, G. Madariaga, A. Kirov, and H. Wondratschek, Zeitschrift für Kristallographie - Crystalline Materials **221**, 15 (2006), URL <https://doi.org/10.1524/zkri.2006.221.1.15>.
  - [51] M. I. Aroyo, A. Kirov, C. Capillas, J. M. Perez-Mato, and H. Wondratschek, Acta Crystallographica Section A **62**, 115 (2006), URL <https://doi.org/10.1107/S0108767305040286>.
  - [52] M. I. Aroyo, J. M. Perez-Mato, D. Orobengoa, E. Tasci, G. de la Flor, and A. Kirov, Bulg. Chem. Commun **43**, 183 (2011).
  - [53] P. J. Brown, V. Nunez, F. Tasset, J. B. Forsyth, and P. Radhakrishna, Journal of Physics: Condensed Matter **2**, 9409 (1990), URL <https://doi.org/10.1088/0953-8984/2/47/015>.
  - [54] P. Liu, J. Li, J. Han, X. Wan, and Q. Liu, Phys. Rev. X **12**, 021016 (2022), URL <https://link.aps.org/doi/10.1103/PhysRevX.12.021016>.
  - [55] S. Zhang, H. Sheng, Z.-D. Song, C. Liang, Y. Jiang, S. Sun, Q. Wu, H. Weng, Z. Fang, X. Dai, et al., Chin. Phys. Lett. **40**, 127101 (2023), website at <https://www.vasp2kp.com/>, URL <https://dx.doi.org/10.1088/0256-307X/40/12/127101>.
  - [56] P. Burlet, F. Bourdarot, J. Rossat-Mignod, J. Sanchez, J. Spirlet, J. Rebizant, and O. Vogt, Physica B: Condensed Matter **180-181**, 131 (1992), ISSN 0921-4526, URL <https://www.sciencedirect.com/science/article/pii/S092145269290683J>.
  - [57] M. M. Hirschmann, A. S. Gibbs, F. Orlandi, D. Khalyavin, P. Manuel, V. Abdolazimi, A. Yaresko, J. Nuss, H. Takagi, A. P. Schnyder, et al., Phys. Rev. Mater. **6**, 114202 (2022), URL <https://link.aps.org/doi/10.1103/PhysRevMaterials.6.114202>.



### Appendix A: Prove the factor system arising from the translation part

Let  $\mathcal{O}_\alpha = \{U_\alpha || R_\alpha | \mathbf{v}_\alpha\}$ ,  $\mathcal{O}_\beta = \{U_\beta || R_\beta | \mathbf{v}_\beta\}$  and  $\mathcal{O}_\gamma = \{U_\alpha U_\beta || R_\alpha R_\beta | (R_\alpha \mathbf{v}_\beta + \mathbf{v}_\alpha) \bmod 1\}$ . We aim to verify that the translation-derived factor takes the form

$$\omega_\tau(\mathcal{O}_\alpha, \mathcal{O}_\beta) = \exp[-i\mathbf{k} \cdot (R_\alpha - \det(U_\alpha))\mathbf{v}_\beta], \quad (\text{A1})$$

and to show how this factor arises from the relation between linear and projective representations.

We relate the projective representation  $M$  and the linear representation  $D$  by a translational phase factor:

$$D(\mathcal{O}_\alpha) = \exp(-i\mathbf{k} \cdot \mathbf{v}_\alpha) M(\mathcal{O}_\alpha). \quad (\text{A2})$$

Using the usual multiplication law for the linear representations,

$$D(\mathcal{O}_\alpha)D(\mathcal{O}_\beta) = D(\{U_\alpha U_\beta || R_\alpha R_\beta | R_\alpha \mathbf{v}_\beta + \mathbf{v}_\alpha\}), \quad (\text{A3})$$

one expects the projective representations to satisfy a modified multiplication rule with a factor system,

$$M(\mathcal{O}_\alpha)M(\mathcal{O}_\beta) = \omega_\tau(\mathcal{O}_\alpha, \mathcal{O}_\beta)M(\mathcal{O}_\gamma), \quad (\text{A4})$$

We now derive  $\omega_\tau$  by substituting Eq. (A2) into the product  $M(\mathcal{O}_\alpha)M(\mathcal{O}_\beta)$ . When  $\mathcal{O}_\alpha$  is unitary (so that  $\det(U_\alpha) = 1$ ), a straightforward manipulation yields

$$\begin{aligned} M(\mathcal{O}_\alpha)M(\mathcal{O}_\beta) &= \exp[i\mathbf{k} \cdot (\mathbf{v}_\alpha + \mathbf{v}_\beta)] D(\mathcal{O}_\alpha)D(\mathcal{O}_\beta) \\ &= \exp[i\mathbf{k} \cdot (\mathbf{v}_\alpha + \mathbf{v}_\beta)] D(\mathcal{O}_\gamma) \exp[-i\mathbf{k} \cdot (R_\alpha \mathbf{v}_\beta + \mathbf{v}_\alpha - \mathbf{v}_\gamma)] \\ &= \exp[i\mathbf{k} \cdot (\mathbf{v}_\alpha + \mathbf{v}_\beta)] M(\mathcal{O}_\gamma) \exp[-i\mathbf{k} \cdot \mathbf{v}_\gamma] \exp[-i\mathbf{k} \cdot (R_\alpha \mathbf{v}_\beta + \mathbf{v}_\alpha - \mathbf{v}_\gamma)] \\ &= \exp[i\mathbf{k} \cdot (\mathbf{v}_\beta - R_\alpha \mathbf{v}_\beta)] M(\mathcal{O}_\gamma) \end{aligned} \quad (\text{A5})$$

from which the unitary case of Eq. (A1) follows.

When  $\mathcal{O}_\alpha$  is anti-unitary (so that  $\det(U_\alpha) = -1$ ), one must account for the fact that both  $M(\mathcal{O}_\alpha)$  and  $D(\mathcal{O}_\alpha)$  reverse the sign of  $i$ , *i.e.*,  $M(\mathcal{O}_\alpha)i = -iM(\mathcal{O}_\alpha)$  and  $D(\mathcal{O}_\alpha)i = -iD(\mathcal{O}_\alpha)$ . Repeating the same substitution and keeping track of this sign change leads to

$$\begin{aligned} M(\mathcal{O}_\alpha)M(\mathcal{O}_\beta) &= \exp[i\mathbf{k} \cdot (\mathbf{v}_\alpha - \mathbf{v}_\beta)] D(\mathcal{O}_\alpha)D(\mathcal{O}_\beta) \\ &= \exp[i\mathbf{k} \cdot (\mathbf{v}_\alpha - \mathbf{v}_\beta)] \exp[-i\mathbf{k} \cdot (R_\alpha \mathbf{v}_\beta + \mathbf{v}_\alpha - \mathbf{v}_\gamma)] D(\mathcal{O}_\gamma) \\ &= \exp[i\mathbf{k} \cdot (\mathbf{v}_\alpha - \mathbf{v}_\beta)] \exp[-i\mathbf{k} \cdot (R_\alpha \mathbf{v}_\beta + \mathbf{v}_\alpha - \mathbf{v}_\gamma)] \exp[-i\mathbf{k} \cdot \mathbf{v}_\gamma] M(\mathcal{O}_\gamma) \\ &= \exp[-i\mathbf{k} \cdot (\mathbf{v}_\beta + R_\alpha \mathbf{v}_\beta)] M(\mathcal{O}_\gamma) \end{aligned} \quad (\text{A6})$$

This yields the anti-unitary case of Eq. (A1).

Combining Eqs. (A5) and (A6), we have thus shown that any linear representation  $D(\mathcal{O}_\alpha)$  obeying Eq. (A3) can be obtained from a projective representation  $M(\mathcal{O}_\alpha)$  that satisfies Eq. (A4) with the factor system given in Eq. (A1). The two representations are related by the translational phase factor in Eq. (A2).

### Appendix B: ‘tbody.in’ parameters

For the tight-binding Hamiltonian, the `tbody.in` is needed. An example of  $\text{Mn}_3\text{Sn}$  with a type-II configuration is given below.

```
spinpol = False
#hr_name_up = sp.up_hr.dat
#hr_name_dn = sp.dn_hr.dat
hr_name = symm_hr.dat

proj:
orbt = 2
spincov = 1
ntau = 8
```

```

0.838800 0.677599 0.250000 2.598077 1.5 0 1 5 ! x1,x2,x3,m1,m2,m3,itype,iorbit
0.161200 0.838800 0.750000 -2.598077 1.5 0 1 5
0.838800 0.161200 0.250000 -2.598077 1.5 0 1 5
0.161200 0.322401 0.750000 2.598077 1.5 0 1 5
0.322401 0.161200 0.250000 0.000000 -3.0 0 1 5
0.677599 0.838800 0.750000 0.000000 -3.0 0 1 5
0.333333 0.666667 0.250000 0.000000 0.0 0 2 3
0.666667 0.333333 0.750000 0.000000 0.0 0 2 3
end proj

kpoint:
kmesh = 10
Nk = 2
0 0 0
0.5 0 0
end kpoint

unit_cell:
5.665000 0.000000 0.000000
-2.832500 4.906034 0.000000
0.000000 0.000000 4.531000
end unit_cell

```

1. **spinpol**: whether the magnetism of the system is collinear (type-I SSG) (*e.g.* ‘ISPIN=2’ and ‘NON-COLLINEAR=.FALSE.’ in INCAR for VASP). Default: **False**.
2. **hr\_name**: the name of the input file containing TB parameters, whose format should be the same as ‘wannier90\_hr.dat’ generated by Wannier90. This parameter only works when **spinpol=False**.
3. **hr\_name\_up**: the name of the input file containing TB parameters with up spin. This parameter is valid for **spinpol=True**.
4. **hr\_name\_dn**: the name of the input file containing TB parameters with down spin. This parameter is valid for **spinpol=True**.
5. **unit\_cell**:  $3 \times 3$  lattice matrix in Cartesian coordinates (Å). Each row is one direct lattice vector, in the order **a**, **b**, **c**. The 3-5 lines in POSCAR can be pasted here directly.
6. **kpoint ... end kpoint**: defines a  $k$ -space path for band sampling.
  - **kmesh**: number of evenly spaced samples taken on each consecutive line segment between listed  $k$ -nodes.
  - **Nk**: number of  $k$  points that follow; the path is formed by connecting them in order.
  - $k$  points list:  $k$  points given in fractional coordinates with respect to the reciprocal basis vectors **b**<sub>1</sub>, **b**<sub>2</sub>, **b**<sub>3</sub>.
7. **proj: ... end proj**: defines the local-orbital projectors used to build the TB basis. Each projector line has eight fields (**x1**, **x2**, **x3**, **m1**, **m2**, **m3**, **itype**, **iorbit**).
  - **orbt**: convention for orbital ordering. It selects how each **iorbit** maps to concrete orbitals, as in Table S1.
  - **spinconv**: *spinful basis ordering*. 1 = orbit-major, spin-minor ( $a \uparrow, b \uparrow, \dots, a \downarrow, b \downarrow, \dots$ ); 2 = spin-major, orbit-minor ( $a \uparrow, a \downarrow, b \uparrow, b \downarrow, \dots$ ).
  - **ntau**: number of site lines that follow (*i.e.*, the number of TB sites listed in this block).
  - Site lines: each line is (**x1**, **x2**, **x3**, **m1**, **m2**, **m3**, **itype**, **iorbit**) where **x1**, **x2**, **x3** are fractional coordinates, **m1**, **m2**, **m3** are magnetic moments in Cartesian coordinates, **itype** labels the atomic species/type, and **iorbit** selects the on-site orbital set according to **orbt** (see Table S1).

Table S1: Local orbitals ordering in different conventions.

iorbit	Convention 1	Convention 2
1	$s$	$s$
3	$p_x, p_y, p_z$	$p_z, p_x, p_y$
5	$d_{xy}, d_{yz}, d_{xz}, d_{x^2-y^2}, d_{z^2}$	$d_{z^2}, d_{xz}, d_{yz}, d_{x^2-y^2}, d_{xy}$
4	$s, p_x, p_y, p_z$	$s, p_z, p_x, p_y$
6	$s, d_{xy}, d_{yz}, d_{xz}, d_{x^2-y^2}, d_{z^2}$	$s, d_{z^2}, d_{xz}, d_{yz}, d_{x^2-y^2}, d_{xy}$
8	$p_x, p_y, p_z, d_{xy}, d_{yz}, d_{xz}, d_{x^2-y^2}, d_{z^2}$	$p_z, p_x, p_y, d_{z^2}, d_{xz}, d_{yz}, d_{x^2-y^2}, d_{xy}$
9	$s, p_x, p_y, p_z, d_{xy}, d_{yz}, d_{xz}, d_{x^2-y^2}, d_{z^2}$	$s, p_z, p_x, p_y, d_{z^2}, d_{xz}, d_{yz}, d_{x^2-y^2}, d_{xy}$
7	$f_{xyz}, f_{5x^3-xr^2}, f_{5y^3-yr^2}, f_{5z^3-zr^2}, f_{x(y^2-z^2)}, f_{y(z^2-x^2)}, f_{z(x^2-y^2)}$	$f_{z^3}, f_{xz^2}, f_{yz^2}, f_{z(x^2-y^2)}, f_{xyz}, f_{x(x^2-3y^2)}, f_{y(3x^2-y^2)}$